Journal of Theoretical Biology 537 (2022) 111005

Contents lists available at ScienceDirect

Journal of Theoretical Biology

journal homepage: www.elsevier.com/locate/yjtbi

Theoretical evidence of osteoblast self-inhibition after activation of the genetic regulatory network controlling mineralization

Abdennasser Chekroun [a,b,1], Laurent Pujo-Menjouet [b,1,*], Steve Falcoz [b,c,2], Kamyine Tsuen [c,e,2], Kevin Yueh-Hsun Yang [d,2], Jean-Philippe Berteau [c,d,e,1]

[a] Laboratoire d'Analyse Non Linéaire et Mathématiques Appliquées, University of Tlemcen, Chetouane 13000, Algeria
[b] Univ Lyon, Inria, Université Claude Bernard Lyon 1, CNRS UMR5208, Institut Camille Jordan, F-69603 Villeurbanne, France
[c] Department of Physical Therapy, College of Staten Island, City University of New York, New York, NY 10314, USA
[d] New York Center for Biomedical Engineering, City College of New York, City University of New York, New York, NY 10031, USA
[e] Nanoscience Initiative, Advance Science Research Center, City University of New York, New York, NY 10031, USA

ARTICLE INFO

Article history:
Received 21 April 2021
Revised 23 December 2021
Accepted 3 January 2022
Available online 12 January 2022

Keywords:
Bone
Genetic network
Nonlinear differential equations
Hill functions

ABSTRACT

Bone is a hard-soft biomaterial built through a self-assembly process under genetic regulatory network (GRN) monitoring. This paper aims to capture the behavior of the bone GRN part that controls mineralization by using a mathematical model. Here, we provide an advanced review of empirical evidence about interactions between gene coding (i) transcription factors and (ii) bone proteins. These interactions are modeled with nonlinear differential equations using Michaelis-Menten and Hill functions. Compared to empirical evidence - coming from osteoblasts culture -, the two best systems (among $12^6 = 2,985,984$ possibilities) use factors of inhibition from the start of the activation of each gene. It reveals negative indirect interactions coming from either negative feedback loops or the recently depicted micro-RNAs. The difference between the two systems also lies in the BSP equation and two ways for activating and reducing its production. Thus, it highlights the critical role of BSP in the bone GRN that acts on bone mineralization. Our study provides the first theoretical evidence of osteoblast self-inhibition after activation of the genetic regulatory network controlling mineralization with this work.

1. Introduction

Bone is a biomaterial made of a soft matrix of collagen (type 1), a hard phase of mineral (carbonated Hydroxyapatite, cAp), and several non-collagenous proteins with water (Bala and Seeman, 2015; Boskey, 1989; Currey, 2013; Granke et al., 2015; Morgan et al., September 2015). For building bone structure, bone cells initiate a self-assembly process monitored by the bone genetic regulatory network (GRN). Although evidence has already well described the main GRN components, their behavior and the order they act on each other for controlling mineralization remain unclear (Fisher and Franz-Odendaal, 2012; Hojo et al., 2016; Xu et al., 2021). Thus, this lack of knowledge is one of the major limitations for developing new treatment when bone's composition is altered by growth and aging (*e.g.* Osteoporosis), genetics disorders (*e.g.* Osteogenesis Imperfecta), or orthopedics issues (*e.g.* joint arthroplasty) (Berteau, 2013; Berteau et al., 2015; Boivin and Meunier, 2003; Currey, 1979; Currey and Butler, 1975; Osterhoff et al., 2016; Younsi et al., 2011; Zioupos and Currey, 1998).

This paper aims to capture the behavior of the bone GRN portion that controls mineralization. We hypothesized that the genetic control of bone mineralization follows a system of nonlinear differential equations to regulate the interactions between the genes of (i) transcription factors and (ii) bone proteins. To do so, we first provided a review of empirical evidence coming from *in* and *ex-vivo* experiments about bone composition and self-assembly process, and *in vitro* experiments about bone GRN and its canonical pathway of activation. We depicted the direct interactions between the genes coding for the transcription factors and those coding for the bone proteins (*e.g.* enhancers or inhibitors of mineralization). Second, we proposed a theoretical behavior of the bone GRN using a system of nonlinear differential equations modeling interactions through Michaelis-Menten and Hill functions. We investigated several mathematical regulation scenarios and compared our *in silico* data to recent *in vitro* data - coming from osteoblasts culture (Sun et al., 2018). In Section 4, we showed that only

* Corresponding author.
E-mail address: pujo@math.univ-lyon1.fr (L. Pujo-Menjouet).
URL: http://math.univ-lyon1.fr/pujo/ (L. Pujo-Menjouet).
[1] These authors contributed equally to this work
[2] These authors contributed equally to this work.

https://doi.org/10.1016/j.jtbi.2022.111005
0022-5193/

two regulatory pathways are possible in theory. While we revealed the need for negative indirect interactions coming from either negative feedback loops or micro-RNAs, we also pointed out the missing experiments needed to complete bone GRN description.

2. Empirical Behavior

2.1. Bone composition and self-assembly process

The soft bone phase is an assembly of crosslinked tropocollagen molecules built through the expression of two central genes, Col1a and LOX. While Col1a codes for tropocollagen molecules, LOX codes for Lysyl-Oxidase, the enzyme facilitates their crosslinking for stiffening a soft matrix (Berteau et al., 2015; Depalle et al., 2018; Rosell-García et al., 2019; Rosell-García and Rodríguez-Pascual, 2020). The hard bone phase originates from the process of mineralization, which consists of the precipitation of Calcium (Ca) and Phosphate (Pi) ions into cAp crystals within the soft matrix of crosslinked tropocollagen (Bala et al., 2013; Boivin and Meunier, 2003; Hosseini et al., 2019; Iline-Vul et al., 2020). This process is regulated through the expression of genes coding for mineralization enhancers (*e.g.* Bone Sialoproteine [BSP], Alkaline Phosphatase [ALP]), and mineralization inhibitors (Osteocalcin [OC] and Osteopontin [OPN]) (Boskey, 1989; Morgan et al., September 2015; Schweighofer et al., 2016).

2.2. Canonical pathway of activation of the bone GRN

The canonical pathway of bone formation is when bone matrix stiffness activates the WNT-β cathenin pathway (Wingless/Beta Catenin pathway) to initiate bone mineralization (Chekroun et al., 2018; Komori, 2011; Mullen et al., 2013; Robling and Turner, 2009; Yavropoulou and Yovos, 2016). For instance, the WNT-β cathenin pathway activates transcription factors (*i.e.* sequence-specific DNA-binding factors) having the ability to inhibit or activate RNA polymerase to bind the promoter gene. Indeed, as they bind the DNA, transcription factors can be activators by calling the RNA polymerase to bind the promoter and start transcription, or inhibitors by blocking the RNA polymerase to bind the promoter and prevent transcription from starting. Like every gene-regulatory network, regulatory components in the bone GRN are thought to contain specific interaction sites for critical regulatory factors. Long-term evidence (Mollentze et al., 2021; Karsenty, 2008; Hartmann, 2009; Licini et al., 2019) depicted the following succession of gene activation: Col1a – ALP – OPN – OC with mineralization starting at OC secretion. More recent evidence shows (i) upregulation of OPN and Col1a at the proliferation stage (Depalle et al., 2021), (ii) upregulation of Col1a, ALP, and BSP at the extracellular matrix maturation (Amarasekara et al., 2021), and (iii) upregulation of OC and OPN at the extracellular matrix mineralization (Ikegame et al., 2019). About this, multiple lines of evidence show that RUNX2 (runt-related transcription factor 2) is the earliest transcription factor that is essential for bone formation (Fisher and Franz-Odendaal, 2012).

Previous evidence has established links for gene activation regarding mineralization enhancers and inhibitors (*e.g.* Col1a, LOX, BSP, ALP, OC, and OPN) and the main bone GRN transcription factors (RUNX2; OSX, Osterix also called Sp7; SATB2, special AT-rich binding component) (Huang et al., 2007; Sharma et al., 2021). More precisely, ALP, BSP, and Col1a are early osteoblast differentiation markers, while OC appears late, concomitantly with mineralization. In addition, OPN peaks twice, during proliferation and then again in the later stages of differentiation (Alakpa et al., 2016; Bouleftour et al., 2016; Dobreva et al., 2006; Gordon et al., 2007; Gordon et al., 2007; Hu et al., 2015; Hu et al., 2015; Klein et al., 2018; Li et al., 2018; Li et al., 2018; Schweighofer et al., 2016; Stepicheva and Song, 2016; Sun et al., 2018; Tang et al., 2011; Tu et al., 2008; Valverde et al., 2008). We integrated the information gathered in Table 1 for the part before BSP and in Table 2 for the part after BSP. Our review shows that BSP acts directly on OPN, OC, and ALP and triggers positive feedback on OSX and RUNX2. Our review suggests that BSP has a central role in the mineralization pathway. We propose a condensed, simple, and version of the bone GRN involved in the mineralization of the bone matrix. Although our version includes the most straightforward pathway without taking feedback loops and double activation into account, we used these actions for discussing our results and interpreting factors of degradation or inhibition (see 4).

We summarized the process as follows: canonical pathway (*e.g.* WNT-β catenin pathway activated by stiffness) triggers bone mineralization through mechanotransduction. This means that bone cell mechanoreceptors stimulation activates the first bone GRN transcription factor (RUNX2). RUNX2 turns then up the production of another transcription factor called OSX, which activates SATB2. SATB2 starts the output of the first enhancers of mineralization (BSP). It induces both the second enhancers (ALP) and the two inhibitors (OC and OPN) of bone mineralization. Thus, our review highlights the central role of BSP in the process presented in Fig. 1.

Table 1
Empirical evidence regarding activation pathways of the bone GRN before mineralization stage.

Element 1		Element 2	Observations	Model	Ref.
Stiffness	+	RUNX2	40 kPa stimulate RUNX2	*in vitro* cell culture	Alakpa et al. (2016)
Stiffness	+	RUNX2	62–68 kPa stimulate RUNX2, ALP, and OPN	*in vitro* cell culture	Sun et al. (2018)
RUNX2	+	OSX	RUNX2 and OSX both increased from early to late stage osteo-differentiation	*in vitro* cell culture	Li et al. (2018)
RUNX2	+	OSX	RUNX2 master regulator upstream of OSX	*in vitro* cell culture	Klein et al. (2018)
OSX	+	SATB2	SATB2 expression is suppressed in the absence of OSX and enhanced when OSX is overexpressed	*in vitro* cell culture	Tang et al. (2011)
SATB2	+	BSP	SATB2 binds to the BSP promoter and regulates BSP expression	*in vitro* cell culture	Tang et al. (2011)
SATB2	+	ALP	overexpression of SATB2 increased ALP activity	*in vitro* cell culture	Hu et al. (2015)
SATB2	+	OC	overexpression of SATB2 increased OC level	*in vitro* cell culture	Hu et al. (2015)
SATB2	+	RUNX2	overexpression of SATB2 increased RUNX2 activity	*ex vivo* Knockout Mice	Dobreva et al. (2006)
downregulation SATB2	–	OC	OC expression is reduced 43-fold	*ex vivo* Knockout Mice	Dobreva et al. (2006)
downregulation SATB2	–	BSP	BSP expression is reduced 5-fold	*ex vivo* Knockout Mice	Dobreva et al. (2006)

Table 2
Empirical evidence regarding activation pathways of the bone GRN after mineralization stage.

Element 1		Element 2	Observations	Model	Ref.
high BSP	+	OPN	high concentration did modeste OPN upregulation	*in vitro* cell culture	Klein et al. (2018)
lack of BSP	+	OPN	downregulation BSP upregulate OPN	*ex vivo* Knockout Mice	Bouleftour et al. (2016)
BSP	+	OC	Baseline expression of OC is higher in BSP +/+	*ex vivo* Knockout Mice	Bouleftour et al. (2015)
Low BSP	–	ALP	Low concentration of BSP downregulates ALP	*in vitro* cell culture	Klein et al. (2018)
High BSP	–	OC	OC levels were lower in serum samples of transgenic	*ex vivo* Knockout Mice	Valverde et al. (2008)
High BSP	=	OC	Continuous addition of exogenous BSP was not sufficient to increase OC	*in vitro* cell culture	Gordon et al. (2007)
High BSP	+	OSX	Continuous addition of exogenous BSP was sufficient to increase OSX	*in vitro* cell culture	Gordon et al. (2007)
High BSP	+	RUNX2	Continuous addition of exogenous BSP was sufficient to increase RUNX2	*in vitro* cell culture	Gordon et al. (2007)
High BSP	–	ALP	ALP levels were lower in serum samples of transgenic	*ex vivo* Knockout Mice	Valverde et al. (2008)

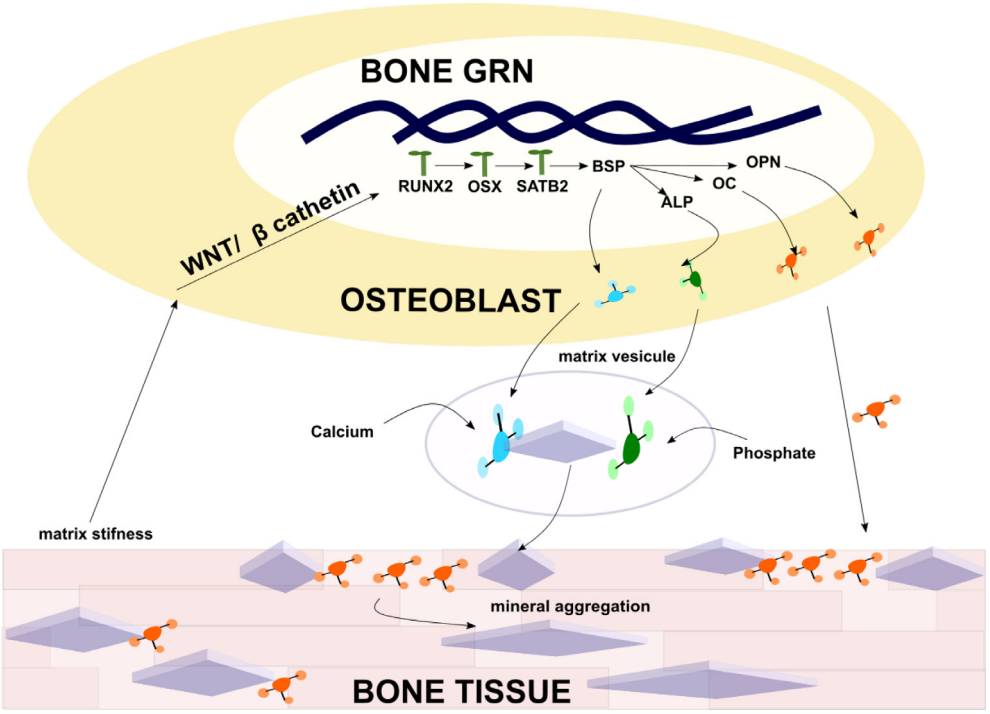

Fig. 1. Condensed version of the bone genetic regulatory network (GRN) that directly acts on mineralization (i.e. production of the bone proteins responsible for bone mineralization). Here, matrix stiffness activates the WNT-β cathenin pathway (mechanotransduction) for initiating the cascade of transcription factor production (RUNX2, OSX, SATB2) that induces production and exocytosis of mineralization enhancers (ALP and BSP) and inhibitors (OC and OPN).

3. Theoretical behavior

3.1. Mathematical model: a multiple-choice approach

According to the condensed bone GRN depicted in Section 2.2, a similar sequence is repeated following the same pattern. The aim of this section is to introduce the general structure of each equation of our GRN model. To that purpose, we use, only here, the generic following notations that will be adapted to each chemical reaction of the model thereafter in the next section. Each equation of the model will show the interaction of two substances x and y. We give an example of a couple of substances at the end of this section. We base our construction in the generic scheme represented in Fig. 2. We insist on the fact that this general process will then be apply specifically to all the key actors of the GRN process. Following Fig. 2, a substance y (in red in the left part of the figure (denoted A) has been previously produced and will start interacting with a substance x (in blue in the center of the figure (denoted P1). We will specify in the next section that substance y needs to reach a certain level of production to trigger production of substance x. This production can be controlled by two possible processes: interaction with micro-RNA (green in the center of the figure (denoted P3) or self-inhibition of substance x (blue dotted array denoted P2 in the figure). We will explain in the next section also how this mechanisms can slow down production of x. Each equation of the model focuses on the production of x, assuming that substance y has been produced and described in the previous equation. To describe every single equation, one of the most frequently used deterministic approaches consists in ordinary differential equations (ODEs), which are based on the law of mass action, that is the production rate of a substance x depends on its balance between its production (gain) and its degradation (loss).

In other words,

x' = gain – loss.

We proposed the following generic mathematical model, which will be specified for every key actors of the GRN following a multiple-choice approach that we set up as a decision tool with three objectives: (i) confirming the biological assumptions based on observed experiments, (ii) rejecting or accepting possible interaction pathways for missing data, and (iii) forecasting the regula-

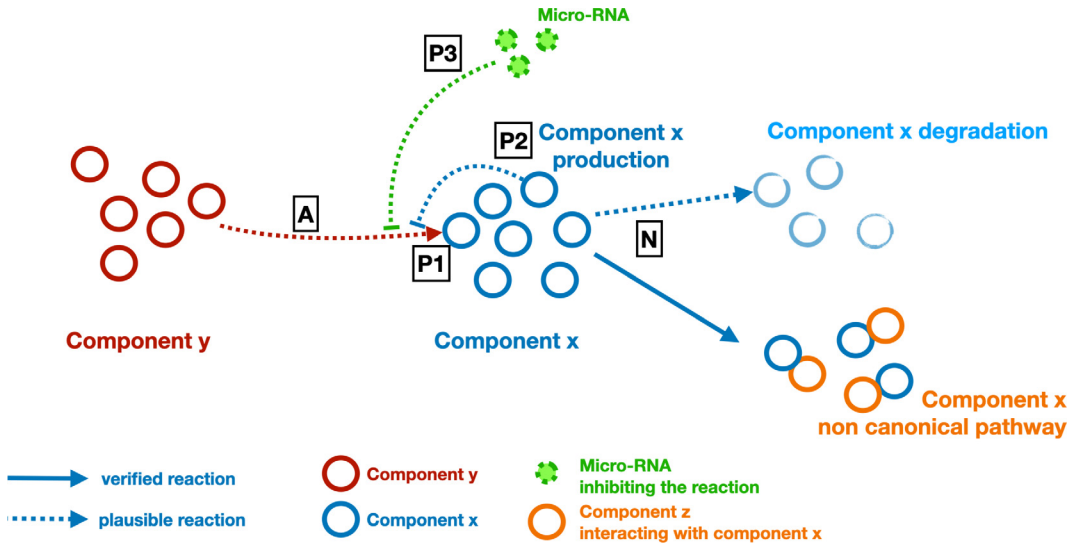

Fig. 2. Schematic representation of a component x production (general formulation). Step 1 (A): through a plausible kinase cascade, component y activates component x production. Step 2: This production can be component y dependent only (P1) with the possible action of component x without action of micro-RNAs (P2) or with their action (P3). Step 3 (N): component x may interact through a non canonical pathway with other component (not studied here) and a plausible degradation. Interaction and degradation are considered as loss terms for the ongoing x canonical interaction. One example in our study is: OSX (transcription factor; component y) activates (process P1) the production of SATB 2 (transcription factor; component x) that is used to activate BSP production. One micro-RNA can act negatively on the production of BSP.

tion system based on a specific stiffness to eventually prevent early pathological formations. To achieve these objectives, we structured the right-hand side of each equation in two parts: a positive term, standing for a growing part due to the component x production from the GRN and a negative term describing its degradation or loss by the binding to one or several (still) unknown components. The consequence of this loss was a decrease in the component concentration. To model our assumptions for each equation of the system, we used the following general form:

$$x' = f(x) - g(x), \tag{1}$$

where f is the positive part, involving an increase (but, to the best of our knowledge saturating) in time of component x (production) and $-g$ is the negative part involving the decrease of x (degradation/binding) (see Fig. 2 for the schematic representation of component x production mechanism). In the next section, x will stand for: WNT-β cathenin, RUNX2, BSP, OC, OPN and ALP components (described in the previous section), while f and g will change their name in each equation depending on which substance is involved. For instance, if the equation describes the production of *RUNX*2, then x will be replaced by *RUNX*2, the role played by y will be replaced by the substance produced just before by the previous reaction, in that case, *WNT* (see Fig. 1 for details). Furthermore, since f and g related directly to *RUNX*2 in this example, they will be denoted f_{RUNX2} and g_{RUNX2} as long as no specific expression of f and g have been identified for this particular equation, then replaced immediately by an explicit form as soon as the best scenario has been selected (after analysis and numerical simulations) (see the Section 3.4.1 for the details of the scenario selection and validation).

3.2. Interpretation of the right-hand sides of generic Eq. (1)

3.2.1. Positive terms f involving an increase in time of component x (production)

Each positive term of the equations describing a concentration increase (steps 1 and 2 in Fig. 2 (see the legend for more details)) may be due to the interaction with other components in presence – for instance, OSX would depend on the RUNX2 concentration. Because, each production is saturated and may be triggered with possible lag time, we decided to propose Hill-like functions f in three different forms: (i) general denoted f_H (H standing for Hill), (ii) not saturating denoted (f_{NS}, NS standing for not saturating), and (iii) with decreasing terms denoted f_{DT} (DT standing for decreasing terms).

(i) General form f_H: Hill function with an extra slowdown term a

In literature, Hill functions are known to describe kinase cascades, or receptor-activator interactions with a low decreasing slope at the early stage, that could be considered as too low concentration (here denoted x as in Fig. 2, steps P1 and P2) to trigger the reaction. Then, a sudden increase in concentration x occurs, ending eventually with a saturation part because f is getting close to 0 when x is large (see Fig. 3). In our model, we add an extra slowdown process enhancing the decelerating part by a specific interaction with the components slowing down the natural process. This term may be interpreted as the micro-RNAs interactions with the component x (see P3 of Fig. 2), leading to a slower production of this latter. In the equation, it appears as a multiplicative constant a in the Hill function form as below (see an example of the extra saturating process influence on the function in Fig. 3). The standard form of this Hill-like function is

$$f_H(x) = k\frac{y^n}{y^n + ax^n}, \tag{2}$$

where x is the concentration of the studied component, y is the concentration of the component interacting with x. Parameters k and n are positive real numbers describing respectively the saturation level and the sensitivity term.

Then at the early stage of the component x production, if the level of the component y (see A and P1 of Fig. 2) about to interact with x is high enough (*i.e.* $y^n \gg ax^n$), then y^n is almost equal to $y^n + ax^n$ and $f_H(x) \approx k$. This gives at the starting point a constant production of component x. But, as x increases, $y^n + ax^n$ becomes larger, and the value of $k\frac{y^n}{y^n+ax^n}$ decreases, which can be interpreted as a saturating growth of component x. And when component y is degraded, y

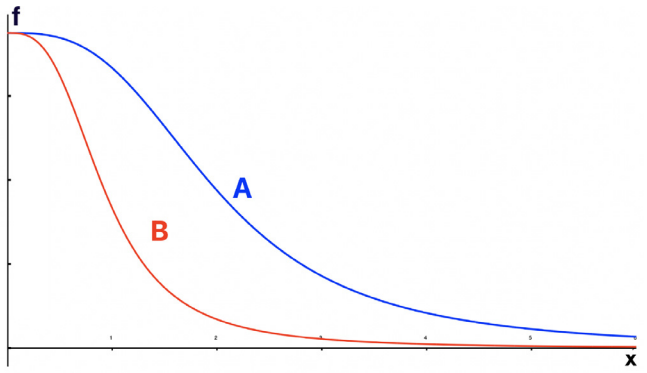

Fig. 3. Hill like function $x \mapsto f_H(x) = k\frac{y^n}{y^n+ax^n}$, where $k = 3, y = 2, n = 3$ and $a = 1$ (graph A), $a = 10$ (graph B). The influence of a is to slow the reaction down (slope is steeper when a is larger).

tends to zero, and thus $k\frac{y^n}{y^n+ax^n}$ tends to zero as x keeps being produced, which stops production of component x too.
Note that:

– if $n = 1$ and $a = 1$, function f_H stands for the well known Michaelis-Menten interaction,
– if $a = 1$, function f_H is the classic Hill function, with no extra-saturating term (see Fig. 3 for the influence on the function and step P1 in Fig. 2 for a biological representation). Saturation still exists as it is a part of the Hill function, but it is not weighted by the extra term a. Note at this point that if $n > 1$, the larger n is, the larger the slope at the triggering time is (very fast reaction when the concentration threshold is reached).

(ii) Non saturating form f_{NS}: a simpler function, called non saturating form, consists in the previous Hill-like function in which, variable x has been replaced by a constant. In that case, x components do not play a saturating role, and its production is y-dependent only, following an exponential increasing pace (see step A in Fig. 2). This variation of the Hill-like function, denoted f_{NS} (u standing for unsaturated), is as follows

$$f_{NS}(x) = k\frac{y^n}{y^n + a}. \tag{3}$$

Thus, when considering Eq. (1) with such a function and no negative term, if component y concentration remains constant, production of component x increases exponentially. On the other hand, if component y concentration increases, production of component x reaches its maximal increasing slope k.

(iii) Decreasing term form f_{DT} : to describe a decreasing production rate in function of components y (step 3 in Fig. 2), we used a form with a decreasing term. We denote f_{DT}, such a function, with d standing for decreasing. This function is defined as follows,

$$f_{DT}(x) = k\frac{1}{y^n + ax^n}. \tag{4}$$

This form shows a much stronger impact on the self-decrease of component x (it is also illustrated by step P3 in Fig. 2). Within this scope, we decide also to investigate the x component independent decreasing function denoted f_{IDT} (step P1 in Fig. 2), and defined by

$$f_{IDT}(x) = k\frac{1}{y^n + a}. \tag{5}$$

3.2.2. Negative terms $-g$ involving the decrease of x (degradation/ binding)

Each negative term of the equation describing a concentration decrease may be due to physiological degradation or binding to other components (corresponding to step N in Fig. 2). We tested three plausible biological assumption: (i) a constant degradation means that the component's continuous use – to either activate the following component or build the bone matrix – is independent of the stiffness (i.e. there is no positive or negative feedback loop in the time frame we studied), (ii) stiffness-dependent loss (degradation or noncanonical pathway) means that the component is more used – to either activate the following component or build the bone matrix- as the matrix stiffness increase (i.e. there is a negative feedback loop from the stiffness in the time frame we studied), and (iii) inverse-stiffness-dependent loss means that the component is less used – to either activate the following component or build the bone matrix- as the matrix stiffness increase. (i.e. there is a positive feedback loop from the stiffness in the time frame we studied). Thus, we propose three different forms of negative terms for Eq. (1): (i) basic loss term denote g_{BL} (BL standing for basic loss), (ii) negative dependence on the source term g_{ND} (ND standing for negative dependence), and (iii) inverse dependence on the source term g_{ID} (ID standing for inverse dependence) that are described as follow:

(i) basic loss term:

$$-g_{BL}(x) = -\mu x, \tag{6}$$

where μ is a positive real value, and x is the component concentration.

(ii) negative dependence on the source term (*i.e.* on matrix stiffness E_y):

$$-g_{ND}(x) = -\mu E_y x. \tag{7}$$

This means that loss increases with the increasing stiffness. This could be biologically explained by the fact that for larger stiffness, components x are more degraded or recruited by other interactions not described in detail for the mineralization process or other bone regulation.

(iii) inverse dependence on the source term (*i.e.* inverse matrix stiffness E_y):

$$-g_{ID}(x) = -\frac{\mu}{E_y}x. \tag{8}$$

This assumption implies that the loss term decreases as the stiffness increases meaning that loss by degradation or non pathological pathway is larger for the early phase, when stiffness is low.

3.3. The full model

To summarize, if we denote the W_N for WNT, R_U for RUNX2, B_S for BSP, O_P for OPN, O_C for OC and A_L for ALP (which are the components defined in Fig. 1) we end up with the following generic system of ordinary differential equations (note that the term generic is due to the fact that at this point, f and g are just the general gain and loss functions of described in Eq. (1).

$$\begin{cases} W_N' &= f(W_N) &- g(W_N), \\ R_U' &= f(R_U) &- g(R_U), \\ B_S' &= f(B_S) &- g(B_S), \\ O_P' &= f(O_P) &- g(O_P), \\ O_C' &= f(O_C) &- g(O_C), \\ A_L' &= f(A_L) &- g(A_L). \end{cases} \tag{9}$$

Two important remarks need to be given at this point. First, every concentration from W_N to A_L are time dependent functions, and for the seek of clarity of the autonomous model we do not mention the variable t. Second, each equation had to be mathematically and biologically investigated in order to choose among each gain functions f (that is one function between f_H, f_{NS}, f_{DT} and f_{IDT}) and each loss functions g (that is one function between g_{BL}, g_{ND} and g_{ID}). To do so, we had to simulate different scenarios. This process is explained in the next subsection.

3.4. Investigating different model scenarios

Our model (9) consists in 6 equations, each of them being written as mentioned in the previous subsection. We investigated several kinetic saturation scenarios based on our review, recent experimental data (Sun et al., 2018), and the well-known chemical interactions studies from Michaelis-Menten and Hill (Ferrell, 1996; Ferrell, 1997; Michaelis and Menten, 1913) – standard to describe saturating process showing possible lag times – for proposing a model that consists in six ordinary differential equations standing for regulation of WNT-β cathenin, RUNX2, BSP, OC, OPN and ALP (see Fig. 1).

To select the most appropriate model, the same set of parameters has to fit the experimental data obtained with three stiffness E_y values: 14.5, 50.5 and 65 Pa. With six equations for the system, four possible positive terms and three possible negative terms, there are $12^6 = 2,985,984$ possible models. We separated thus our models in two parts: (i) the WNT-β cathenin and RUNX2 equations and (ii) the BSP, OPN, OC, ALP equations and we used the least square method (see the Supplementary Material file Section 3 for details).

3.4.1. Selection and validation of scenarios for WNT-β cathenin and RUNX2

For WNT-β cathenin and RUNX2 equations, two selections of terms among 144 possibilities were suitable (see Fig. 4). Our results show that two distinct subgroups fitted correctly the data. Their main differences rely on the influence of the inhibition factor: first row of simulations is with a_W and a_R values about 1 for unsaturated and saturated models, while in the second row,a_W and a_R values are respectively 69.6 and 122.7 for unsaturated and saturated models. In other words, one subgroup (first row of simulations of Fig. 4) is simulated with a_W and a_R (A) (micro-RNA influence) values about 1 while in the second row (B), a_W and a_R (see systems (10) and (11) for the equations of the models) play an important role with values respectively of 69.6 and 122.7. The other values are given in the legend of figure Fig. 4) At this stage of simulation, it is thus impossible to claim that the inhibition factor is crucial in the process and only new biological investigations on their influence could allow us to differentiate one set of parameter from another one. We had to test both to see if we reached saturation or not. Our results presenting no differences between both

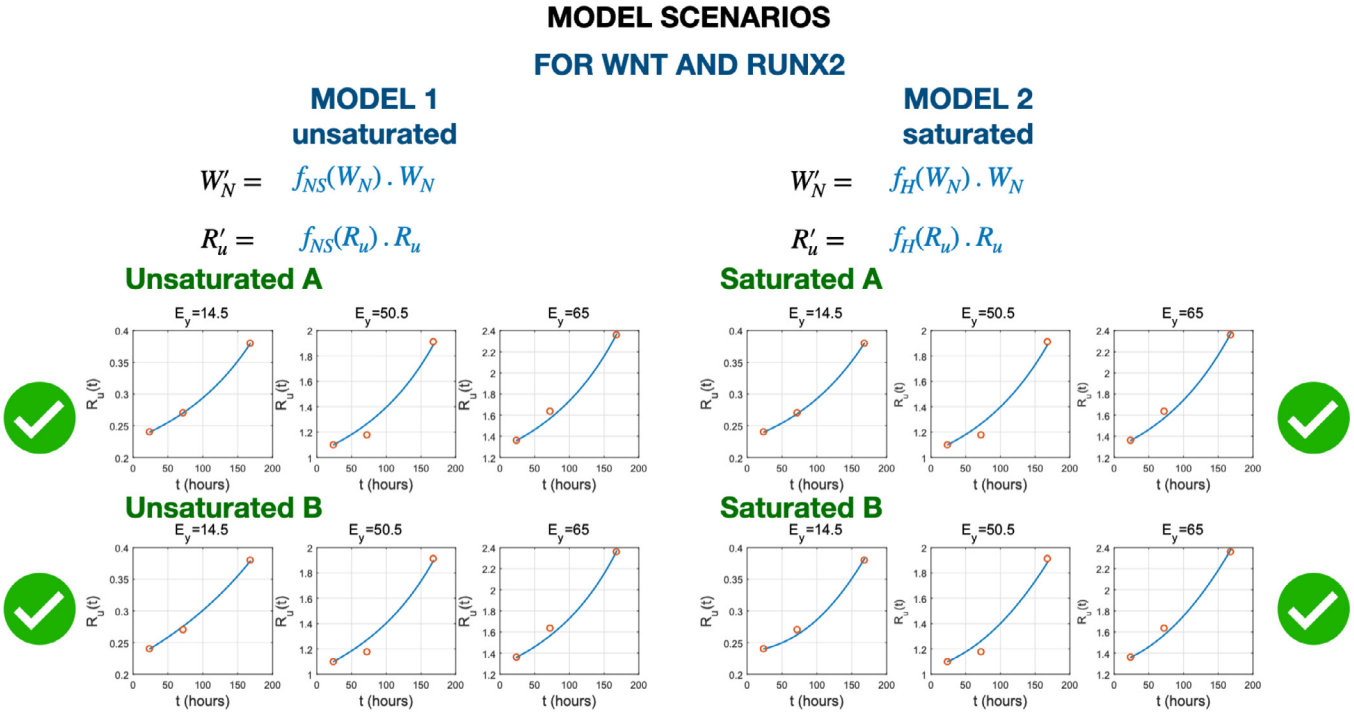

Fig. 4. After a literature review, and experimental data fitting, we came up with a selection of four possible models among 144 possible ones. Their main differences rely on the influence of the inhibition factor: first row of simulations is with a_W and a_R values about 1 for unsaturated and saturated A models, while in the second row, a_W and a_R values are respectively 69.6 and 122.7 for unsaturated and saturated B. Values are the following: **unsaturated A** ($k_1 = 0.0059, a_w = 1.0006, k_2 = 0.0248, a_R = 0.9981, \nu_w = 1.0078, \nu_R = 0.9949$), **unsaturated B** ($k_1 = 0.0100, a_w = 69.6016, k_2 = 0.8392, a_R = 122.7328, \nu_w = 1.0477, \nu_R = 1.0004$), **saturated A** ($k_1 = 0.0100, a_w = 0.9865, k_2 = 0.0186, a_R = 0.7748, \nu_w = 0.7000, \nu_R = 0.9964$), **saturated B** ($k_1 = 0.0430, a_w = 270.5291, k_2 = 0.6448, a_R = 100.0059, \nu_w = 1.0139, \nu_R = 1.0002$). Experimental plots are taken at 24 h, 72 h and 168 h.

Table 3
Variables and parameters used in the models and their description. Note that all variables W_N, R_U, B_S, O_P, O_C and A_L depend on the time t, and all the parameters are non negative constants.

Variables	Description
W_N	WNT-β concentration
R_U	RUNX2 concentration
B_S	BSP concentration
O_P	OPN concentration
O_C	OC concentration
A_L	ALP concentration
Parameters	**Description**
E_y	Stiffness
k_i, $i = 1, \dots, 6$	Saturation levels for each concentration
$\mu_{B_S}, \mu_{O_P}, \mu_{O_C}, \mu_{A_L}$	Degradation rate or interaction through a non canonical pathway with other component
$\nu_W, \nu_R, \nu_{B_S}, \nu_{O_P}, \nu_{O_C}, \nu_{A_L}$	Sensitivity constants of Hill functions
$a_W, a_R, a_{B_S}, a_{O_P}, a_{O_C}, a_{A_L}$	Saturating weight due to micro-RNA

conditions suggest that the bone GRN is not saturated for that range of stiffness. However, we took the arbitrary choice to pick up the saturated model for two reasons: 1- give the whole system the homogeneous saturated form, and 2- to give a door open for future experimental results that may need to add microRNA impact in these two equations.

This will be more investigated in our next objective: when we get the whole feedback loop with mineralization increasing continuously the stiffness. This closed system will then be biologically investigated, and the role of microRNA even more particularly. At this stage, we admit that this is arbitrary only but open enough to give biologists freedom to include it or not (taking all the a_W ora_R equal to 1 Consequently, since only one model (the model 2 of Fig. 4) was in agreement with the biological inhibition hypothesis (a Hill function for the gain and no loss function). We then used model 2 with saturated B assumption for running simulations of the entire model and we described it in the next subsection.

3.4.2. Selection and validation of scenarios for BSP, OSX, OPN, OC

All the parameters of the model are non negative constants, and they are described in Table 3. For BSP, OSX, OPN and OC equations, after tedious investigations, two selections of terms (case 1b and case 3a (see Fig. 5)) among $12^4 = 20,736$ possibilities appeared suitable for us. We describe them in the two following scenarios:

1. Scenario 1b:

$$\begin{cases} W_N' &= k_1 \frac{E_y^{\nu_W}}{E_y^{\nu_W} + a_W W_N^{\nu_W}} W_N, \\ R_U' &= k_2 \frac{W_N^{\nu_R}}{W_N^{\nu_R} + a_R R_U^{\nu_R}} R_U, \\ B_S' &= k_3 \frac{R_U^{\nu_{B_S}}}{R_U^{\nu_{B_S}} + a_{B_S} B_S^{\nu_{B_S}}} B_S - \mu_{B_S} B_S, \\ O_P' &= k_4 \frac{1}{B_S^{\nu_{O_P}} + a_{O_P} O_P^{\nu_{O_P}}} O_P - \frac{\mu_{O_P}}{E_y} O_P, \\ O_C' &= k_5 \frac{B_S^{\nu_{O_C}}}{B_S^{\nu_{O_C}} + a_{O_C} O_C^{\nu_{O_C}}} O_C - \mu_{O_C} O_C, \\ A_L' &= k_6 \frac{1}{B_S^{\nu_{A_L}} + a_{A_L} A_L^{\nu_{A_L}}} A_L - \frac{\mu_{A_L}}{E_y} A_L. \end{cases} \tag{10}$$

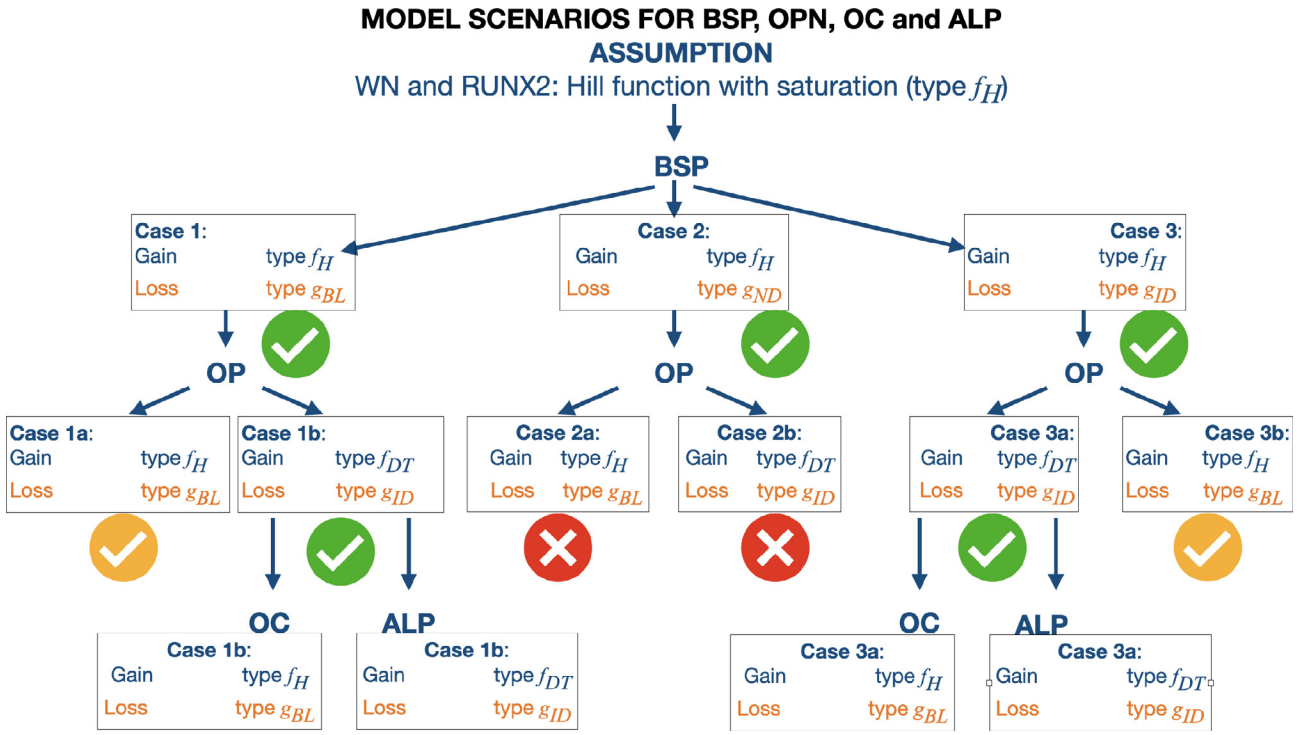

Fig. 5. Selecting the best fitted model among the 20,736 possibilities. Only two candidates were chosen: case 1b and case 3a. Other cases were tested but could not fit data.

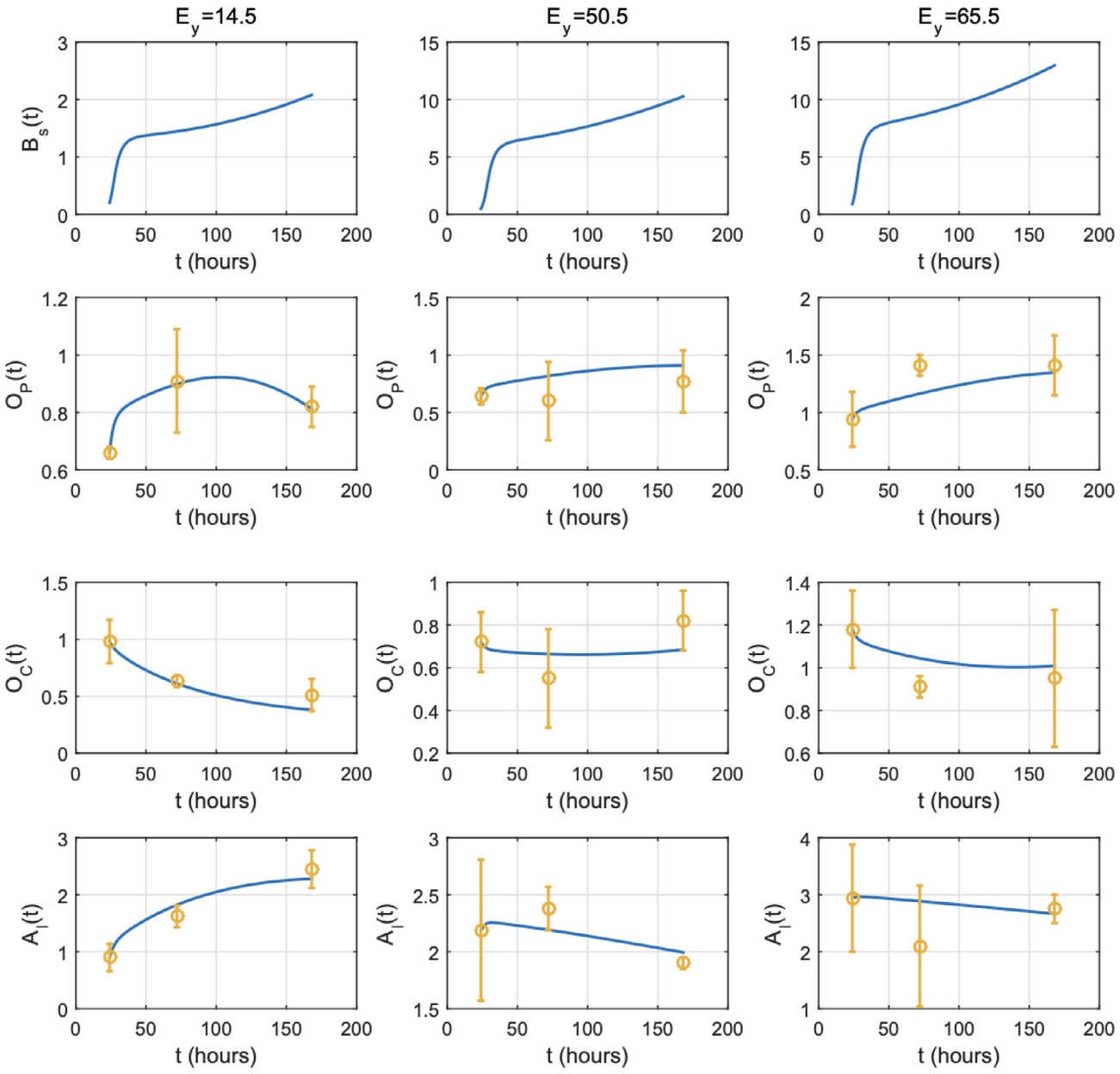

Fig. 6. The selected model based scenario 1b: parameter values are $k_3 = 0.4993, a_{B_S} = 0.0353, v_{B_S} = 2.8123, k_4 = 0.0339, a_{O_P} = 0.0061, v_{O_P} = 0.6692, k_5 = 0.0557, a_{O_C} = 0.5819, v_{O_C} = 0.5292, k_6 = 0.0668, a_{A_L} = 0.8857, v_{A_L} = 2.5820, \mu_{B_S} = 0.0922, \mu_{O_P} = 0.3587, \mu_{O_C} = 0.0480, \mu_{A_L} = 0.0641$. Experimental plots are taken at 24 h, 72 h and 168 h.

2. Scenario 3a:

$$\begin{cases} W_N' &= k_1 \frac{E_y{}^{v_W}}{E_y^{v_W} + a_W W_N^{v_W}} W_N, \\ R_U' &= k_2 \frac{W_N{}^{v_R}}{W_N^{v_R} + a_R R_U^{v_R}} R_U, \\ B_S' &= k_3 \frac{R_U{}^{v_{B_S}}}{R_U^{v_{B_S}} + a_{B_S} B_S^{v_{B_S}}} B_S & - \frac{\mu_{B_S}}{E_y} B_S, \\ O_P' &= k_4 \frac{1}{B_S^{v_{O_P}} + a_{O_P} O_P^{v_{O_P}}} O_P & - \frac{\mu_{O_P}}{E_y} O_P, \\ O_C' &= k_5 \frac{B_S^{v_{O_C}}}{B_S^{v_{O_C}} + a_{O_C} O_C^{v_{O_C}}} O_C & - \mu_{O_C} O_C, \\ A_L' &= k_6 \frac{1}{B_S^{v_{A_L}} + a_{A_L} A_L^{v_{A_L}}} A_L & - \frac{\mu_{A_L}}{E_y} A_L. \end{cases} \tag{11}$$

The resulting simulations are given in Fig. 6 for scenario 1*b* and in Fig. 7 for scenario 3*a*.

Remark: to give a comparison, we added simulations that do not fit in the Supplementary Material Section 2. Moreover, our source codes for simulations are available on demand to the correspondent author.

4. Discussion

Although evidence has already proposed several theoretical approaches to bone mineralization and remodeling, none of them address the bone GRN behavior (Buenzli, 2015; Isaksson et al., 2008; Rieger et al., 2011). Here, we detailed the role played by each production of transcription factors, enhancers, and inhibitors of mineralization. We used the canonical pathway of bone GRN acti-

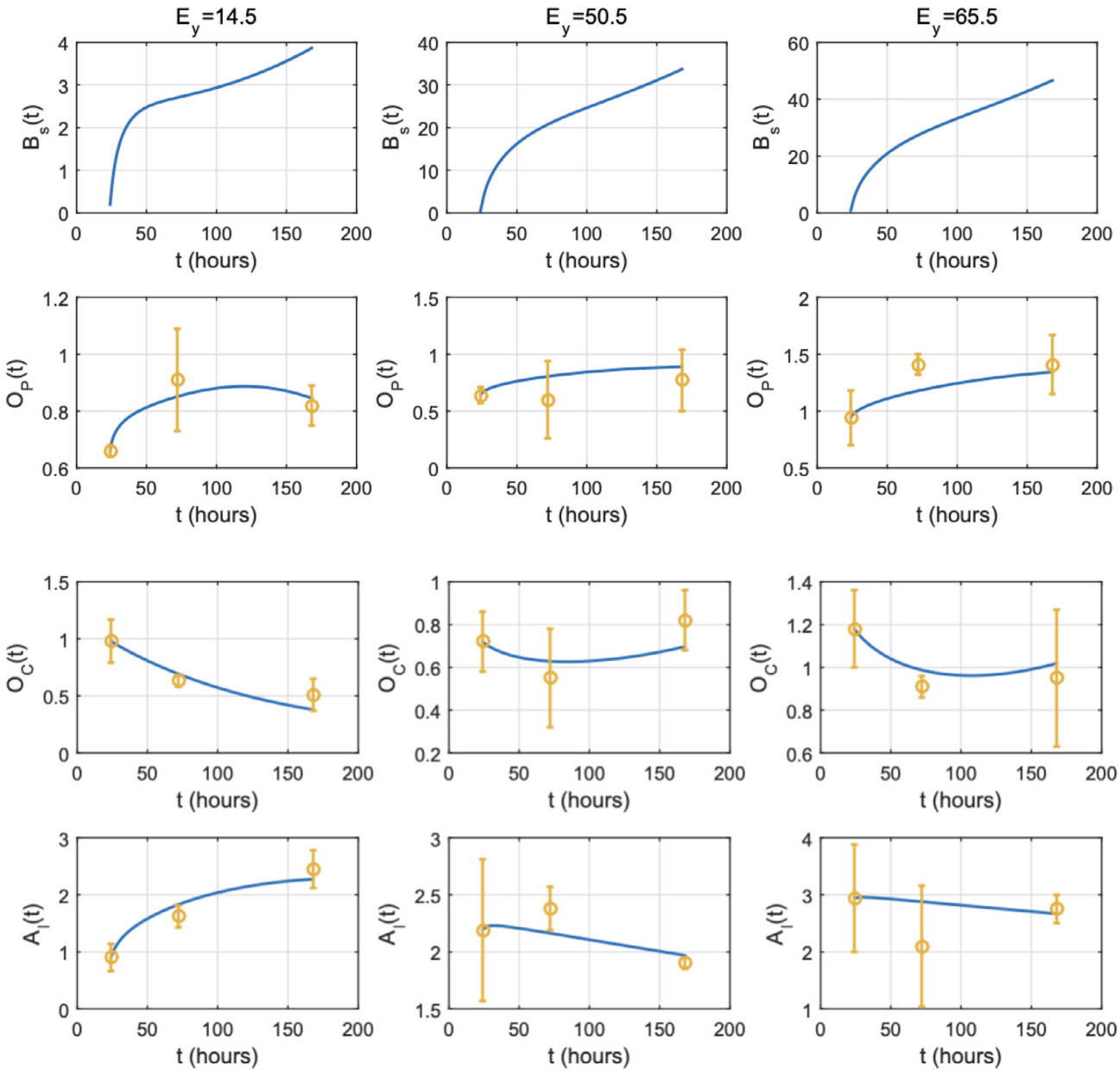

Fig. 7. The selected model based scenario 3a: parameter values are $k_3 = 1.9994, a_{B_S} = 0.4244, \upsilon_{B_S} = 1.9053,\ k_4 = 0.0371, a_{O_P} = 0.0025, \upsilon_{O_P} = 0.5078, k_5 = 0.0924, a_{O_C} = 299.9984, \upsilon_{O_C} = 0.9350, k_6 = 0.4847, a_{A_L} = 7.7552, \upsilon_{A_L} = 2.7359,\ \mu_{B_S} = 0.7398, \mu_{O_P} = 0.3000, \mu_{O_C} = 0.0080, \mu_{A_L} = 0.0531$. Experimental plots are taken at 24 h, 72 h and 168 h.

vation (Wingless/Beta Catenin) and modeled transcription factors and bone protein production through Michaelis-Menten and Hill function. As a result, we proposed two nonlinear differential equations that fit well with the experimental data. The two best systems used an inhibition factor in each equation modeling each element of the bone GRN, showing the theoretical evidence of bone GRN inhibition during bone mineralization through stiffness matrix evolution. The difference between the two systems lies in the BSP equation and two ways for activating and reducing its production. Thus, it highlights the critical role of BSP in the bone GRN that acts on bone mineralization.

For instance, our predictions show that case 1b and case 3a were the only relevant results (see Fig. 5) for BSP, OSX, OPN, and OC production (see models 10 and 11). In these models, the favorable terms of production, based on well-known modeling of kinetic interaction through the Hill-like functions, provided results that fit our experimental data only with Hill functions adding a slow down parameter – or a decreasing function with saturation. These results indicate that the weighting coefficient a (amplification factor) of formula 2 plays a significant role in fitting the data. Although further sensitivity analyses of saturation are necessary to depict the range of acceptable values, our data support the existence of a saturation level for the components' production involved in bone mineralization. In addition, in the two most accurate models, the negative terms of production (degradation) provided results that fit our experimental data only with constant degradation term g_{BL} or stiffness inversely dependence term g_{ID}. Constant degradation g_{BL} is when the negative term μ is independent of any other interaction (see Fig. 6)). On the other hand, g_{ID} is used when the loss term decreases as stiffness increases. The best fits to experimental data finally happened when inhibition action on degradation is inversely proportional to the stiffness when the loss term

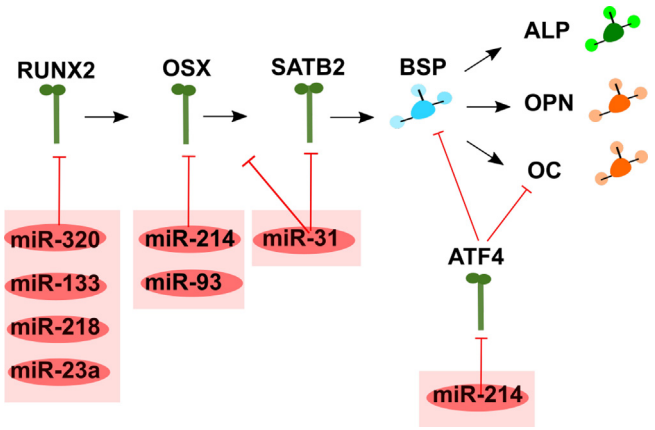

Fig. 8. samples of micro-RNAs in the bone GRN pathway for controlling mineralization.

is function g_{ID}. In this paper, we had to compare our theoretical research to empirical research that employed hydrogels with variable stiffnesses for modulating the mechanical environment of cells. Thus, mechanotransduction (*i.e.*, WNT-β catenin regulation) had to be our primary source of bone GRN activation. This constraint made our model-independent of other osteogenic signals (*e.g.*, coming from osteoclasts). Thus, by comparing our in silico results to *in vitro* results – coming from cell culture of osteoblasts-, we depict for the first time an osteoblast self-inhibition without the action of osteoclasts.

As mentioned in the material and method section, we tested three plausible biological assumptions: (i) a constant degradation, (ii) a stiffness-dependent loss (degradation or noncanonical pathway), and (iii) an inverse-stiffness-dependent loss. The (ii) stiffness-dependent loss (degradation or noncanonical pathway) hypothesis seemed to be the most relevant because it induces a negative feedback loop from the stiffness that could correspond to the initiation of the bone remodeling. However, our simulations showed that the best scenario used hypothesis (iii) that implies an inverse-stiffness-dependent loss. It means that the component is less used – to either activate the following component or build the bone matrix- as the matrix stiffness increase. It means that there is a positive feedback loop from the stiffness on the osteoblasts in the time frame we studied. Thus, we may investigate several assumptions in the future: (i) degradation may play a secondary role as it may be a slow process (as shown in the increasing experimental data between time 24 h, 72 h, and 168 h) or (ii) stiffness influence is so low that it does not influence degradation at this stage of the experiment. Although we could investigate more low stiffness samples or degradation of the two starter terms (WNT and RUNX2), our data support the lack of direct negative dependence on the source term (see the simulations of WNT and RUNX2 with degradation in the Supplementary Material Section 1 and note that this does not change anything in comparison with simulations shown in Fig. 4).

Regarding limitations of the method used here, there is a wide choice of optimal, statistical, and machine learning methods such as kriging or gradient descent that can help to validate the best set of parameters. However, we need more time-series data points for using them. Thus, our following goals are to (i) obtain BSP data sets (missing in our work here) and (ii) describe a complete feedback loop between transcription factors and matrix stiffness both with experimental observations and theoretical predictions. Although in physiological conditions, several factors from the extracellular and ecological aspects of bone mineralization impact the bone GRN (*e.g.*, Transforming growth factor-beta, Oncostatin M, or Bone morphogenetic proteins), our research disregards the role of bone-resorbing osteoclasts and the associated osteogenic signals. In future research, we will integrate these parameters when seeking to model *in vivo* behavior and, more specifically, bone remodeling.

In our results, we found that an extra saturation term is necessary. We suggest that extra saturation could result from miRNA's action. For instance, MiRNAs are small non-coding RNA molecules that regulate the post-transcriptional gene expression by inhibiting target mRNA translations or promoting transcript degradation. Regarding bone, miRNAs are the core of complex circuits involving components of multiple pathways for promoting or inhibiting osteogenesis. In addition, evidence has shown that all pathways converge to RUNX2 and SATB2 expression and activation (Komori, 2011), which are transcription factors that represent master regulators responsible for OB differentiation. Thus, miRNAs involved in their downregulation determine osteogenesis inhibition. In addition, a recent review (Bellavia et al., 2019) published an exhaustive overview of miRNAs involved in bone homeostasis and highlighted their possible role in pathological development. Thus, the specific micro RNA of the bone GRN – osteomirs – can fulfill the role of "inhibitor" saturation term a because they modulate epigenetic states in given genomics loci of the bone GRN. Here, instead of proposing one osteomir per genomics locus, we propose a cluster of osteomirs inhibiting each transcription factors that directly modulate the production of both enhancers and inhibitors of mineralization (see Fig. 8). We selected only those whose inhibitory effect on transcription factors promoters was shown in laboratory and clinical studies (linked to human individuals dealing with bone pathologies). For instance, we propose a cluster of osteomirs that directly inhibit RUNX 2 and are related to bone pathologies such as osteoporosis: miR-320 (Yu et al., 2011), miR-133a (Wang et al., 2012), miR-218 (De-Ugarte et al., 2016) and miRNA-23a (Zhao et al., 2014). We also propose another transcription factor called ATF-4 with its regulator mir-214 (Matsuguchi et al., 2009). However, ATF-4 is also able to activate the WNT-β cathenin pathway (Yu et al., 2013). Although it has been shown that osteoblast proliferation and differentiation are likely regulated by reciprocal regulation rather than a cascade of the transcription factor, in this paper, we addressed the regulation of the mineralization part as a linear chain.The manipulation of key gene-regulatory elements, such as disease-associated loci and bone regeneration-associated loci, may be an attractive new approach to gene therapy for genetic disorders and regenerative medicine in skeletal tissues. Our next endeavor will be to integrate another key (positive or negative) feedback loop in our model.

Finally, with the mineralization precursor processes outputs of our model, it might be possible to deduce the number of crystals created according to the number of BSP and ALP present in the extracellular matrix. Indeed, as the two main enhancers of crystal assembly are BSP and ALP, and the two main components of crystals are calcium and phosphate, knowing the number of those four entities should hopefully be able to allow us to forecast the number of crystals created. The concentrations of Calcium and Phosphate necessary to obtain one crystal – based on the ratio Ca/PO4 of 1,67 (Siswanto et al., 2020) – are two inputs for performing mineralization prediction. Consequently, our future work will be to decipher the exact relationship between enhancers of mineralization and molecule concentrations to predict the number of crystals that one cell can produce.

5. Conclusion

We provide the first theoretical evidence of a necessary osteoblast self-inhibition after activation of the genetic regulatory network controlling mineralization. Compared to empirical evidence,

the two best systems used an inhibition factor in each equation modeling each element of the bone GRN. It reveals negative indirect interactions coming from either negative feedback loops or the recently depicted micro-RNAs. The difference between the two systems lies in the BSP equation and two ways for activating and reducing its production. Thus, it highlights the critical role of BSP in the bone GRN that acts on bone mineralization.

CRediT authorship contribution statement

Abdennasser Chekroun: Conceptualization, Methodology, Software, Validation, Formal analysis, Data curation, Writing – original draft, Writing – review & editing, Visualization, Supervision, Project administration. **Laurent Pujo-Menjouet:** Conceptualization, Methodology, Formal analysis, Writing – original draft, Writing – review & editing, Visualization, Supervision, Project administration, Funding acquisition. **Steve Falcoz:** Software, Validation, Writing – original draft. **Kamyine Tsuen:** Investigation. **Kevin Tsueng:** Investigation. **Jean-Philippe Berteau:** Conceptualization, Methodology, Investigation, Data curation, Writing – original draft, Writing – review & editing, Visualization, Supervision, Project administration, Funding acquisition.

Declaration of Competing Interest

The authors declare that they have no known competing financial interests or personal relationships that could have appeared to influence the work reported in this paper.

Acknowledgement

The authors want to thank the “International Network at CSI” for their support regarding international scholar visits. The authors want to thank also the National Institute for Mathematical Sciences and their Interactions (INSMI) from CNRS, the French Ambassy of France in Algeria and the Algerian Ministry of Higher Education and Scientific Research Studies for the Maurice Audin chair related to this research.

Appendix A. Supplementary data

Supplementary data associated with this article can be found, in the online version, athttps://doi.org/10.1016/j.jtbi.2022.111005.

References

Alakpa, E.V., Jayawarna, V., Lampel, A., Burgess, K.V., West, C.C., Bakker, S.C.J., Roy, S., Javid, N., Fleming, S., Lamprou, D.A., Yang, J., Miller, A., Urquhart, A.J., Frederix, P. W.J.M., Hunt, N.T., Péault, B., Ulijn, R.V., Dalby, M.J., 2016. Tunable supramolecular hydrogels for selection of lineage-guiding metabolites in stem cell cultures. Chem 1 (2), 298–319.

Amarasekara, D.S., Kim, S., Rho, J., 2021. Regulation of Osteoblast Differentiation by Cytokine Networks. Int. J. Mol. Sci. 22 (6), 2851.

Bala, Y., Farlay, D., Boivin, G., 2013. Bone mineralization: from tissue to crystal in normal and pathological contexts. Osteoporosis Int. 24 (8), 2153–2166.

Bala, Y., Seeman, E., 2015. Bone’s material constituents and their contribution to bone strength in health, disease, and treatment. Calcif. Tissue Int. 97 (3), 308–326.

Bellavia, D., De Luca, A., Carina, V., Costa, V., Raimondi, L., Salamanna, F., Alessandro, R., Fini, M., Giavaresi, G., 2019. Deregulated miRNAs in bone health: Epigenetic roles in osteoporosis. Bone 122, 52–75.

Berteau, J.-P., 2013. La biomécanique de l’os de l’enfant en croissance, une aide à la prise en charge kinésithérapique. Kinésithérapie, la Revue 13(143), 16–21. Publisher: Elsevier Masson..

Berteau, J.P., Gineyts, E., Pithioux, M., Baron, C., Boivin, G., Lasaygues, P., Chabrand, P., Follet, H., 2015. Ratio between mature and immature enzymatic cross-links correlates with post-yield cortical bone behavior: an insight into greenstick fractures of the child fibula. Bone 79, 190–195.

Boivin, G., Meunier, P.J., 2003. The mineralization of bone tissue: a forgotten dimension in osteoporosis research. Osteoporosis Int. 14 (Suppl 3), S19–24.

Boskey, A.L., 1989. Noncollagenous matrix proteins and their role in mineralization. Bone Min. 6 (2), 111–123.

Bouleftour, W., Bouet, G., Granito, R.N., Thomas, M., Linossier, M.T., Vanden-Bossche, A., Aubin, J.E., Lafage-Proust, M.H., Vico, L., Malaval, L., 2015. Blocking the expression of both bone sialoprotein (bsp) and osteopontin (opn) impairs the anabolic action of pth in mouse calvaria bone. J. Cell Physiol. 230 (3), 568–577.

Bouleftour, W., Juignet, L., Bouet, G., Granito, R.N., Vanden-Bossche, A., Laroche, N., Aubin, J.E., Lafage-Proust, M.-H., Vico, L., Malaval, L., 2016. The role of the sibling, bone sialoprotein in skeletal biology – contribution of mouse experimental genetics. Matrix Biol. 52–54, 60–77.

Buenzli, P.R., 2015. Osteocytes as a record of bone formation dynamics: A mathematical model of osteocyte generation in bone matrix. J. Theor. Biol. 364, 418–427.

Chekroun, A., Pujo-Menjouet, L., Berteau, J.P., 2018. A novel multiscale mathematical model for building bone substitute materials for children. Materials 11 (6).

Currey, J.D., 1979. Changes in the impact energy absorption of bone with age. J. Biomech. 12 (6), 459–469.

Currey, J.D., 2013. Bones structure and mechanics. Princeton University Press, Princeton, NJ. OCLC: 872359669.

Currey, J.D., Butler, G., 1975. The mechanical properties of bone tissue in children. J. Bone Joint Surg. Am. 57 (6), 810–814.

De-Ugarte, L., Yoskovitz, G., Balcells, S., Güerri-Fernández, R., Martinez-Diaz, S., Mellibovsky, L., Urreizti, R., Nogués, X., Grinberg, D., García-Giralt, N., Díez-Pérez, A., 2016. Mirna profiling of whole trabecular bone: identification of osteoporosis-related changes in mirnas in human hip bones. BMC Med. Genomics 8 (1), 75.

Depalle, B., Duarte, A.G., Fiedler, I.A.K., Pujo-Menjouet, L., Buehler, M.J., Berteau, J.-P., 2018. The different distribution of enzymatic collagen cross-links found in adult and children bone result in different mechanical behavior of collagen. Bone 110, 107–114.

Depalle, B., McGilvery, C.M., Nobakhti, S., Aldegaither, N., Shefelbine, S.J., Porter, A.E., 2021. Osteopontin regulates type I collagen fibril formation in bone tissue. Acta Biomater. 120, 194–202.

Dobreva, G., Chahrour, M., Dautzenberg, M., Chirivella, L., Kanzler, B., Fariñas, I., Karsenty, G., Grosschedl, R., 2006. Satb2 is a multifunctional determinant of craniofacial patterning and osteoblast differentiation. Cell 125 (5), 971–986.

Ferrell, J.E., 1996. Tripping the switch fantastic: how a protein kinase cascade can convert graded inputs into switch-like outputs. Trends Biochem. Sci. 21 (12), 460–466.

Ferrell, J.E., 1997. How responses get more switch-like as you move down a protein kinase cascade. Trends Biochem. Sci. 22 (8), 288–289.

Fisher, S., Franz-Odendaal, T., 2012. Evolution of the bone gene regulatory network. Curr. Opin. Genet. Develop. 22 (4), 390–397.

Gordon, J.A.R., Tye, C.E., Sampaio, A.V., Underhill, T.M., Hunter, G.K., Goldberg, H.A., 2007. Bone sialoprotein expression enhances osteoblast differentiation and matrix mineralization in vitro. Bone 41 (3), 462–473.

Gordon, J.A.R., Tye, C.E., Sampaio, A.V., Underhill, T.M., Hunter, G.K., Goldberg, H.A., 2007. Bone sialoprotein expression enhances osteoblast differentiation and matrix mineralization in vitro. Bone 41 (3), 462–473.

Granke, M., Does, M.D., Nyman, J.S., 2015. The role of water compartments in the material properties of cortical bone. Calcif. Tissue Int. 97 (3), 292–307.

Hartmann, C., 2009. Transcriptional networks controlling skeletal development. Curr. Opin. Genet. Develop. 19 (5), 437–443.

Hojo, H., McMahon, A.P., Ohba, S., 2016. An emerging regulatory landscape for skeletal development. Trends Genet. 32 (12), 774–787.

Hosseini, S., Naderi-Manesh, H., Vali, H., Baghaban Eslaminejad, M., Azam Sayahpour, F., Sheibani, S., Faghihi, S., 2019. Contribution of osteocalcin-mimetic peptide enhances osteogenic activity and extracellular matrix mineralization of human osteoblast-like cells. Colloids Surf. B 173, 662–671.

Hu, N., Feng, C., Jiang, Y., Miao, Q., Liu, H., 2015. Regulative effect of mir-205 on osteogenic differentiation of bone mesenchymal stem cells (bmscs): Possible role of SATB2/Runx2 and ERK/MAPK pathway. Int. J. Mol. Sci. 16 (5), 10491–10506.

Hu, N., Feng, C., Jiang, Y., Miao, Q., Liu, H., 2015. Regulative effect of mir-205 on osteogenic differentiation of bone mesenchymal stem cells BMSCs: possible role of SATB2/Runx2 and ERK/MAPK pathway. Int. J. Mol. Sci. 16 (12), 10491–10506.

Huang, W., Yang, S., Shao, J., Li, Y.-P., 2007. Signaling and transcriptional regulation in osteoblast commitment and differentiation. Front. Biosci. 12, 3068–3092.

Ikegame, M., Ejiri, S., Okamura, H., 2019. Expression of Non-collagenous Bone Matrix Proteins in Osteoblasts Stimulated by Mechanical Stretching in the Cranial Suture of Neonatal Mice. J. Histochem. Cytochem. 67 (2), 107–116.

Iline-Vul, T., Nanda, R., Mateos, B., Hazan, S., Matlahov, I., Perelshtein, I., Keinan-Adamsky, K., Althoff-Ospelt, G., Konrat, R., Goobes, G., 2020. Osteopontin regulates biomimetic calcium phosphate crystallization from disordered mineral layers covering apatite crystallites. Scientific Rep. 10 (1), 15722.

Isaksson, H., van Donkelaar, C., Huiskes, R., Ito, K., 2008. A mechano-regulatory bone-healing model incorporating cell-phenotype specific activity. J. Theor. Biol. 252 (2), 230–246.

Karsenty, G., 2008. Transcriptional control of skeletogenesis. Annu. Rev. Genomics Hum. Genet. 9, 183–196.

Klein, A., Baranowski, A., Ritz, U., Gñtz, H., Heinemann, S., Mattyasovszky, S., Rommens, P.M., Hofmann, A., 2018. Effect of bone sialoprotein coated three-dimensional printed calcium phosphate scaffolds on primary human osteoblasts. J. Biomed. Mater. Res. Part B 106 (7), 2565–2575.

Komori, T., 2011. Signaling networks in runx2-dependent bone development. J. Cell. Biochem. 3, 750–755.
Komori, T., 2011. Signaling networks in RUNX2-dependent bone development. J. Cell. Biochem. 112 (3), 750–755.
Li, C., Sunderic, K., Nicoll, S.B., Wang, S., 2018. Downregulation of heat shock protein 70 impairs osteogenic and chondrogenic differentiation in human mesenchymal stem cells. Scientific Rep. 8 (1), 553.
Li, C., Sunderic, K., Nicoll, S.B., Wang, S., 2018. Downregulation of heat shock protein 70 impairs osteogenic and chondrogenic differentiation in human mesenchymal stem cells. Scientific Rep. 8 (1), 553.
Licini, C., Vitale-Brovarone, C., Mattioli-Belmonte, M., 2019. Collagen and non-collagenous proteins molecular crosstalk in the pathophysiology of osteoporosis. Cytokine Growth Factor Rev. 49, 59–69.
Matsuguchi, T., Chiba, N., Bandow, K., Kakimoto, K., Masuda, A., Ohnishi, T., 2009. JNK Activity Is Essential for Atf4 Expression and Late-Stage Osteoblast Differentiation. J. Bone Miner. Res. 24 (3), 398–410.
Michaelis, L., Menten, M.L., 1913. The kinetics of the inversion effect. Biochemische Zeitung 49, 333–369.
Mollentze, J., Durandt, C., Pepper, M.S., 2021. An In Vitro and In Vivo Comparison of Osteogenic Differentiation of Human Mesenchymal Stromal/Stem Cells. Stem Cells Int 2021, 1–23.
Morgan, S., Poundarik, A.A., Vashishth, D., rgan et al., September 2015. Do non-collagenous proteins affect skeletal mechanical properties? Calcif. Tissue Int. 97 (3), 281–291.
Mullen, C.A., Haugh, M.G., Schaffler, M.B., Majeska, R.J., McNamara, L.M., 2013. Osteocyte differentiation is regulated by extracellular matrix stiffness and intercellular separation. J. Mech. Behav. Biomed. Mater. 28, 183–194.
Osterhoff, G., Morgan, E.F., Shefelbine, S.J., Karim, L., McNamara, L.M., Augat, P., 2016. Bone mechanical properties and changes with osteoporosis. Injury 47, 11–20.
Rieger, R., Hambli, R., Jennane, R., 2011. Modeling of biological doses and mechanical effects on bone transduction. J. Theor. Biol. 274 (1), 36–42.
Robling, A.-G., Turner, C.-H., 2009. Mechanical signaling for bone modeling and remodeling. Crit. Rev. Eukaryot Gene Expr. 19 (4), 319–338.
Rosell-García, T., Paradela, A., Bravo, G., Dupont, L., Bekhouche, M., Colige, A., Rodriguez-Pascual, F., 2019. Differential cleavage of lysyl oxidase by the metalloproteinases BMP1 and ADAMTS2/14 regulates collagen binding through a tyrosine sulfate domain. J. Biol. Chem. 294 (29), 11087–11100.
Rosell-García, T., Rodríguez-Pascual, F., 2020. Boosting collagen deposition with a lysyl oxidase/bone morphogenetic protein-1 cocktail. Methods Cell Biol. 156, 259–270.
Schweighofer, N., Aigelsreiter, A., Trummer, O., Graf-Rechberger, M., Hacker, N., Kniepeiss, D., Wagner, D., Stiegler, P., Trummer, C., Pieber, T., Obermayer-Pietsch, B., Müller, H., 2016. Direct comparison of regulators of calcification between bone and vessels in humans. Bone 88, 31–38.
Sharma, V., Srinivasan, A., Nikolajeff, F., Kumar, S., 2021. Biomineralization process in hard tissues: The interaction complexity within protein and inorganic counterparts. Acta Biomater. 120, 20–37.
Siswanto, S., Hikmawati, D., Benecdita, N., Nurmala, S., 2020. Synthesis of hydroxyapatite based on nano coral using precipitation method for bone substitution. J. Phys: Conf. Ser. 1445, 012015.
Stepicheva, N.A., Song, J.L., 2016. Function and regulation of microRNA-31 in development and disease: miR-31 in development and disease. Mol. Reprod. Dev. 83 (8), 654–674.
Sun, M., Chi, G., Li, P., Lv, S., Xu, J., Xu, Z., Xia, Y., Tan, Y., Xu, J., Li, L., Li, Y., 2018. Effects of matrix stiffness on the morphology, adhesion, proliferation and osteogenic differentiation of mesenchymal stem cells. Int. J. Med. Sci. 15 (3), 257–268.
Tang, W., Li, Y., Osimiri, L., Zhang, C., 2011. Osteoblast-specific transcription factor osterix (osx) is an upstream regulator of satb2 during bone formation. J. Biol. Chem. 286 (38), 32995–33002.
Tu, Q., Zhang, J., Paz, J., Wade, K., Yang, P., Chen, J., 2008. Haploinsufficiency of Runx2 results in bone formation decrease and different bsp expression pattern changes in two transgenic mouse models. J. Cell. Physiol. 217 (1), 40–47.
Valverde, P., Zhang, J., Fix, A., Zhu, J., Ma, W., Tu, Q., Chen, J., 2008. Overexpression of bone sialoprotein leads to an uncoupling of bone formation and bone resorption in mice. J. Bone Mineral Res. 23 (11), 1775–1788.
Wang, Y., Li, L., Moore, B.T., Peng, X.-H., Fang, X., Lappe, J.M., Recker, R.R., Xiao, P., 2012. Mir-133a in human circulating monocytes: a potential biomarker associated with ostmenopausal osteoporosis. PLoS ONE 7, (4) e34641.
Xu, F., Li, W., Yang, X., Na, L., Chen, L., Liu, G., 2021. The roles of epigenetics regulation in bone metabolism and osteoporosis. Front. Cell Develop. Biol. 8, 619301.
Yavropoulou, M.P., Yovos, J.G., 2016. Mechanical signaling for bone modeling and remodeling. J. Musculoskeletal Neuronal Interactions 19 (4), 221–236.
Younsi, R., Launay, F., Glard, Y., Berteau, J.-P., Chabrand, P., Bollini, G., 2011. Fracture après allongement des membres inférieurs chez l'enfant: étude d'une série de 96 patients. Revue de Chirurgie Orthopédique et Traumatologique 97(7), S280. Publisher: Elsevier Masson..
Yu, F., Cui, Y., Zhou, X., Zhang, X., Han, J., 2011. Osteogenic differentiation of human ligament fibroblasts induced by conditioned medium of osteoclast-like cells. Bioscience Trends 5 (2), 46–51.
Yu, S., Zhu, K., Lai, Y., Zhao, Z., Fan, J., Im, H.-J., Chen, D., Xiao, G., 2013. ATF4 Promotes β)Catenin Expression and Osteoblastic Differentiation of Bone Marrow Mesenchymal Stem Cells. Int. J. Biol. Sci. 9 (3), 256–266.
Zhao, X., Xu, D., Li, Y., Zhang, J., Liu, T., Ji, Y., Wang, J., Zhou, G., Xie, X., 2014. Micrornas regulate bone metabolism. J. Bone Miner. Metab. 32 (3), 221–231.
Zioupos, P., Currey, J.D., 1998. Changes in the stiffness, strength, and toughness of human cortical bone with age. Bone 22 (1), 57–66.